ATTITUDE DETERMINATION FROM TRIAXIAL ELLIPSOID OF UNKNOWN ORIENTATION

Cody Waldecker

Submitted in Partial Fullfillment of the Requirements
for the Degree of

MASTER OF SCIENCE

Approved by:
Dr. John Christian, Chair
Dr. Kurt Anderson
Dr. John Wen

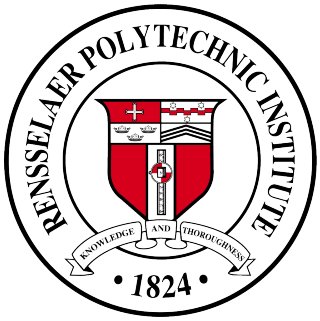

Department of Aeronautical Engineering
Rensselaer Polytechnic Institute
Troy, New York

[December 2020]
Submitted November 2020

CONTENTS

LIST OF FIGURES

ABSTRACT

Presented is the derivation for the rotation matrix describing the principal axis of a celestial body of unknown attitude relative to a spacecraft of known attitude. Through the use of the lit limb of an ellipsoidal body and the body's principal axis, a modified orthogonal Procrustes problem can be solved for attitude determination. Due to the natural symmetry of triaxial ellipsoids, the solution method presents a twofold equivocacy in the attitude of the observed body. In addition, it presents a different method for mapping the quadric surface of an ellipsoidal body to the projection on an image plane. Then, through matrix factorization, the position relative to the celestial body can be derived. The method presented offers an exact solution and avoids the error associated with ellipse fitting an image.

1. INTRODUCTION

As national space organizations continue plans for sending humans beyond Earth's orbit, the demand for improved autonomous spacecraft navigation is ever increasing. This is particularly true when it comes to mission design where a major restriction is having continual contact with Earth-based support. In order to meet this need for autonomous spacecraft navigation, the use of passive observations has been developed over the years. This idea was first applied during NASA's Gemini Program, where astronauts used a space sextant to measure the angle between an apparent horizon and reference stars [1, 2, 3]. The same measurements taken manually by the astronauts may also be determined from an image, leading to the development of image based navigation for robot space exploration missions [4] which was first demonstrated on the Mariner missions to Mars [5]. However, the technique has proven essential for any mission to outer planets.

This method of using images of planets and moons has been utilized for spacecraft navigation in deep space for over 50 years [4]. "Optical Navigation (OPNAV) is the application of narrow-field astrometry to spacecraft orbit determination. In the most basic form, OPNAV pictures of a target body against a background of reference stars provide a measurement of the apparent right ascension and declination of the target as seen from the spacecraft" [4]. These observations provide the only direct data for determining the relative orientation of the spacecraft to the observed celestial body. Using Earth-based astrometry, the spacecraft's heliocentric trajectory (trajectory about the sun), is easily determined. Thus, the optical data measures the third arm of the Sun-spacecraft-Body triangle.

This method of OPNAV, using the images of a planet or a moon, has typically been performed by analysts on Earth. Typically, data and images are sent from the spacecraft to researchers on Earth, who then apply image processing tools to determine the relative attitude of each celestial body captured [6]. Recently, increased research has been dedicated towards eliminating the reliance on Earth based human analysts in the event of a communication system failure [7, 8, 9]. This has given rise to many forms of spacecraft dynamics

determination.

One technique is to use the planet as the central body of examination. There are two prominent OPNAV techniques where celestial bodies are the focal point: those that use landmarks on the body's surface, and those that use the body's illuminated horizon. Landmark techniques require a relatively close range to the body, but tend to produce more accurate results than horizon-based techniques. Therefore, horizon-based methods are typically less accurate than the landmark based counterpart and may be performed from a much larger range. However, horizon-based techniques do not require the use of terrain models or rendering software, which makes them often faster and simpler than landmark techniques [12, 13, 14, 15].

When determining the relative attitude of a spacecraft to an observed body, assuming that the distance between them is great enough that horizon based methods are more desirable than landmark based methods, the combination of horizon and star measurements, called limb-star OPNAV, may be used. However, there are difficulties that arise when trying to process an image in limb-star OPNAV. First, planets and moons appear much brighter than stars in images, making it difficult to properly expose both stars and planets in the same image. Second, it relies on the continual availability of stars. Since autonomous OPNAV is meant as a back-up to Earth-based tracking, if a navigation back-up is being utilized, a failure has already occurred. For example, during Apollo 13 an explosion of an oxygen tank created a field of small debris around the spacecraft. This debris field made it impossible for astronauts to distinguish between debris and distant stars [16]. An autonomous system is likely to encounter the same problem in a similar situation and would not be able to identify stars for navigation.

Therefore, the need for horizon-based OPNAV is evident. The objective of horizon-based OPNAV is to use knowledge of a planets shape and orientation, the attitude of the spacecraft's camera, and line of sight measurements to estimate the relative distance between the spacecraft and the observed planet [18]. Analytically, if the observed body is an ellipsoid where the orientation and size are known, then the rotation can be computed, and the full attitude obtained. This is a well documented topic including iterative and non-iterative techniques [18, 19]. However, previous knowledge of the object's orientation must be known,

such as the axis of rotation.

A frequently used technique for determining spacecraft attitude is through the use of a celestial body's lit limb. The projection of a planet or moon is captured onto a camera's focal plane in the shape of an ellipse, or a circle in few cases. Then, a conic section is derived from the projection and used to calculate dynamics, such as distance to the planet. Section 2.4 presents two different methods for using the captured projection to determine spacecraft distance from a planet. The first will be the currently adopted method and the second will be that of Hartley and Zisserman, who use quadrics for the derivations. Quadrics, or quadric surfaces, are a generalization of conic sections which contain $D-1$ dimensions in a three dimensional Euclidean space. When the defining polynomial of the projection is not absolutely irreducible, homogeneous coordinates can be introduced to define a degenerate quadric. Finally, the degenerate quadric can be used to solve for the conic section and therefore the relative attitude or distance of the observing spacecraft.

The use of ellipse fits, and most OPNAV techniques, rely on the observed body to have a stable orbit and rotation. However, this is not always the case. As will be described in section 2.1, there are some celestial bodies which do not have a stable axis of rotation, called tumbling bodies or described as having a chaotic rotation state. These bodies chaotically rotate in space and require another method for determining spacecraft orientation. Chapter 3 presents a method of using an ellipse fit and perspective geometry to solve a modified orthogonal Procrustes problem. The optimal solution, given by a Frobenius norm minimization, presents a solution of two symmetric rotation matrices which will define the orientation of the celestial body relative to the observing spacecraft.

2. Background

2.1 Geometry of Celestial Bodies

Modern science has made everyone familiar with the concept that planets and moons are nearly perfect spheres. Especially from a great distance, the naked eye can hardly notice that these celestial bodies are not perfectly round. However, through careful examination, it becomes clear that rotating planets are slightly oblate and moons are triaxial [21]. In addition, these celestial bodies all have unique topology such as mountains, craters, and valleys. The tendency of large masses to form spherical shapes was first noted by Isaac Newton in The Mathematical Principles of Natural Philosophy [22]. His insight showed that in the absence of other forces, the gravitational attraction between matter tends to mold bodies into spheres.

Newton himself later recognized the first cause of deviation from a perfect sphere. The rotation of bodies introduces oblateness where the polar radii of planets is smaller than the equatorial radii. He discovered that gravity naturally forms spherical bodies, but it's rotation simultaneously expands their equators. The higher the rotation rate of a celestial body, the more disproportionate its equatorial axes become.

Several hundred years later, Newton's contemporaries managed to discover the next complication in planetary shape, tidal forces [21]. Tides are the result of variations in the gravitational pull of a central body due to the orbit of a satellite. The consequence is that the satellite becomes elongated along the vector between the centers of the bodies. If a satellite, including planets, which are satellites around a star, has a spin rate which is different than it's orbital period, then the elongation of the equipotential surface varies with time [21]. Therefore, a point on the equator alternately raises and lowers as the satellite orbits the central body. These periodic changes are what creates oceanic tides on earth. However, these tides also dissipate rotational energy and, if applied for long enough, will eventually slow the satellites rotation. It is also tidal forces that can be attributed to the formation of

the shape of most bodies in the solar system today, the triaxial ellipsoid.

Tidal forces have been found to effect not only body shape but also the planets spin about it's axis of rotation; where the spin axis coincides with the celestial body's maximum moment of inertia. The moment of inertia is actually a second rank tensor which can be defined for any solid body, and in the case of steady spin bodies, there will be a constant diagonal matrix describing the lowest kinetic energy possible for a fixed angular momentum. When a body finally spins about this stable axis, it cannot further change it's rotation unless acted upon by an external torque.

For typical natural satellites, tidal friction over time will alter its spin to a value proportional to its orbital mean motion, reaching a steady state spin about the maximum moment of inertia. Many satellites have reached this final state including the Moon, the two Martian satellites, and most moons of Saturn [23]. However, there are dramatic exceptions to this general picture, namely Saturn's satellite, Hyperion. For Hyperion, "measures of the exponential rate of separation of nearby trajectories in phase space indicate that the rotation is chaotic and not just a regular motion through large angles" [24]. This can be attributed to the largely oblate shape of the moon, Hyperion. Voyager pictures have shown Hyperion to be significantly out of round, with the long axis roughly twice as long as the short axis [25]. The standard spin-orbit coupling is not valid for a body with such large asphericity [26].

However, Hyperion is not the only example of this chaotic nature. In fact, Giblin and Farinella (1997) discovered that many asteroids involved in an impact will display visible tumbling [27]. But these tumbling asteroids are not as far off as one may think, an example of this can be seen in the Duende asteroid that passed near Earth in 2013. The asteroid experienced an extremely close Earth encounter, within 28,000 km [28]. After an observatory campaign was launched, it was discovered that the asteroid was in a tumbling state before it's encounter with Earth. Then, due to tidal forces, the spin state was altered, however, the asteroid remained in non-principal axis rotation [29].

This tumbling nature has been witnessed in multiple asteroids in the solar system, including Toutalis, Crocus, Seleucus, and Gleuke [30]. In addition, in 1994, Harris [31]

concluded that for several asteroids, the damping time scale to reach a stable spin rate is considerably longer than the age of the Solar System, leading to the large amplitude wobble seen in tumbling bodies.

Although there have been many supporting cases of asteroids and some moons exhibiting tumbling nature, there are likely many more that have not been documented. Therefore, there is an evident need for OPNAV techniques which can be applied to these chaotically rotating bodies. Previous methods of using a body's axis of rotation for calculations are invalid for tumbling bodies due to their unpredictable rotation in space, presenting the need for new, alternative techniques. The work that follows shows potential application for any of these chaotic rotations observed within and beyond our solar system.

2.2 Pinhole Camera Model

If a celestial body is modeled as a triaxial ellipsoid, then the projection on the image plane is formed from the rays that start at the camera and are tangent to the observed horizon of the planet [41]. The assembly of the tangent rays forms the tightly bounding cone around the planet with the vertex at the camera center. If a planar slice of this cone is taken, the planets projection is formed onto the image plane. Therefore, the apparent horizon of the planets conic forms the projection of an ellipse in almost all OPNAV scenarios [18]. In order to accurately describe this, a pinhole camera model is adopted to relate the translation of points in the real world to an image frame.

The pinhole camera model is an idealized image formation method governed by perspective geometry. Real cameras are not pinholes and suffer from distortment issues and imperfections, however, it is reasonable to assume a pinhole camera model in calculations because these imperfections may be corrected via calibrations and present a result equivalent to a pinhole camera [32].

For the basic pinhole camera model in OPNAV, consider the projection of points in space onto a plane. The center of the projection is the origin of the Euclidean coordinate system, the camera center, with the $+Z$ axis pointing along the boresight of the camera

and the projection plane is the focal plane of the camera. Under the pinhole camera model, a point in space with standard Cartesian coordinates is mapped to the point on the image plane where the ray from the point X intersects the focal plane [32]. Defining the focal plane distance as f, the pinhole camera model is given by

$$x_i = f\frac{X_i}{Z_i} \qquad y_i = f\frac{Y_i}{Z_i} \tag{2.1}$$

Where the coordinates $[X_i, Y_i, Z_i]$ correspond to a point on the planet surface in the camera frame, and the coordinates $[x_i, y_i]$ correspond to the same point on the focal plane [33]. This transformation describes the central projection mapping from Euclidean 3D space to Euclidean 2D space. The focal plane point is in units of length and must be converted to pixel coordinates using the camera calibration matrix [34].

Without a loss of generality, the focal length f may be set to 1, to work in focal length normalized coordinates [18]. Therefore, the image plane coordinates may be written in terms of homogeneous coordinates.

$$\begin{bmatrix} x_i \\ y_i \\ 1 \end{bmatrix} = \frac{1}{Z_i} \begin{bmatrix} X_i \\ Y_i \\ Z_i \end{bmatrix} \tag{2.2}$$

It becomes clear that the coordinates of a point on the focal plane occur where the ray from the camera crosses the image plane at $Z = 1$. In addition, this reflects that any point in an image can be used to construct the ray that originates at the camera center in the direction of the observed point.

2.3 Conic Surface Formed by Back Projection of Imaged Ellipse

With basic knowledge of the pinhole model, it can be seen that the ray that emanates from the camera and passes through a point on the projected ellipse, forms a tangent to the

observed celestial body. Therefore, the projected ellipse can be used to derive an equation describing the cone of tangent rays. While there are a variety of existing methods to accomplish this, the method presented by Dr. Christian will prove the most useful here [36]. This proves beneficial because it defines the conic surface entirely in terms of the coefficients of the 2D ellipse. The work that follows is entirely his.

Begin by noting that a referenced planet or moon may be assumed to be a smooth triaxial ellipsoid. The term smooth means that any roughness due to terrain is neglected. This is a reasonable assumption because of the fact that horizon based OPNAV occurs at long distances where surface landmarks are difficult to identify. Given this assumption, it is well known that all spheroids and triaxial ellipsoids project a 2D ellipse when captured by a camera image. Then, the derivation may begin by recalling the implicit equation for a 2D ellipse on an image plane,

$$Ax_i^2 + Bx_iy_i + Cy_i^2 + Dx_i + Fy_i + G = 0 \tag{2.3}$$

where $4AC$ must be greater than B^2 in order for the equation to match that of an ellipse. The derivation of the ellipse coefficients will be neglected here, however, they may be found through use of multiple methods [37]. Now, by substituting Eq.(2.1) into the equation of an ellipse, this ellipse can be related to a conical surface on which the corresponding 3D points must lie.

$$A\left(f\frac{X_i}{Z_i}\right)^2 + B\left(f\frac{X_i}{Z_i}\right)\left(f\frac{Y_i}{Z_i}\right) + C\left(f\frac{Y_i}{Z_i}\right)^2 + D\left(f\frac{X_i}{Z_i}\right) + F\left(f\frac{Y_i}{Z_i}\right) + G = 0 \tag{2.4}$$

$$Af^2X_i^2 + Bf^2X_iY_i + Cf^2Y_i^2 + DfX_iZ_i + FfY_iZ_i + GZ_i^2 = 0 \tag{2.5}$$

This can then be written in matrix-vector form as

$$\begin{bmatrix} X_i & Y_i & Z_i \end{bmatrix} \begin{bmatrix} Af^2 & Bf^2/2 & Df/2 \\ Bf^2/2 & Cf^2 & Ff/2 \\ Df/2 & Ff/2 & G \end{bmatrix} \begin{bmatrix} X_i \\ Y_i \\ Z_i \end{bmatrix} = 0 \tag{2.6}$$

then, $\mathbf{C}$ and $\mathbf{s}_i$ can be defined by the matrices above.

$$\mathbf{C} = \begin{bmatrix} Af^2 & Bf^2/2 & Df/2 \\ Bf^2/2 & Cf^2 & Ff/2 \\ Df/2 & Ff/2 & G \end{bmatrix}, \mathbf{s}_i = \begin{bmatrix} X_i \\ Y_i \\ Z_i \end{bmatrix} \tag{2.7}$$

Therefore, the following must be true at all times,

$$\mathbf{s_i^T C s_i} = 0 \tag{2.8}$$

It can be noted that Eq.(2.8) is the equation for a conical surface. Therefore, all values of $\mathbf{s_i}$ that satisfy the equation form a cone, and at the intersection of the conic section and the camera image plane, an ellipse is projected. If the ellipse on the image plane is the product of a triaxial ellipsoid, then the cone formed by the 2D ellipse on the focal plane must be the same as the cone that tightly bounds the 3D triaxial ellipsoid. This is shown visually in Fig.(2.1) below, where the camera is centered at the origin with coordinates [0 0 0].

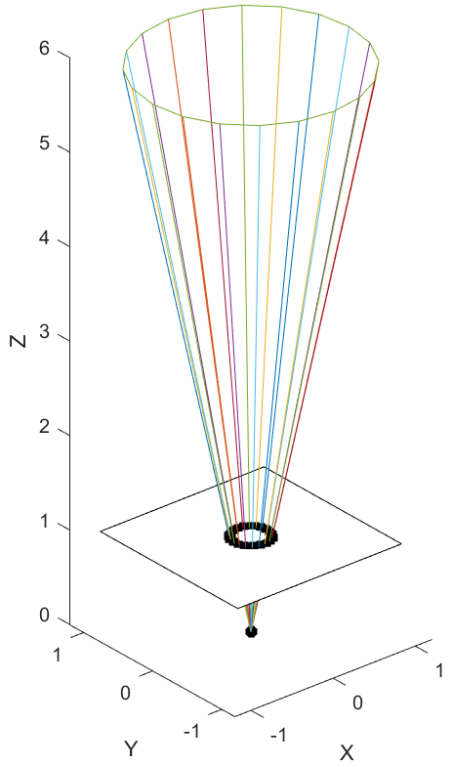

Figure 2.1: Visualization of Conic Projection

It can be seen above that a cone of rays is formed by the 2D ellipse on the image plane at $f = Z = 1$ where the camera is located at the origin. This 2D ellipse can then be used to solve for all values of $\mathbf{s}_i$, which will be used in later calculations.

2.4 Derivation of Tightly Bounding Cone

There is a great deal of literature describing the projection of a triaxial ellipsoid onto an image plane, however, there is much less work available for using a projected ellipse to estimate the location and orientation of a known celestial body. Notable earlier work has been successful at reconstructing spheres [38] and spheroids [39] using multiple images. However, unlike the work to reconstruct an unknown ellipsoid from it's projected ellipse, instead, the goal is to use a single image of a body of known shape and use that to determine the distance or orientation relative to an observing spacecraft. One of the previous components must be know, distance or orientation, in order to calculate the other. However, before calculating

attitude or distance, the projected ellipse must be used to form the equation of the set of rays that tightly bound the observed body.

Two methods will be presented here. The first will be the method created by Dr. Christian [37] and the second will be that of Hartley and Zisserman [33], who use quadrics for the derivations. Both methods are based off of a similar background, which will be described below.

Now, recalling that all triaxial ellipsiods may be assumed to be smooth surfaces in the frame of the camera. Then, the surface of the planet may be described by the quadric equation of an ellipsoid,

$$\frac{x_P^2}{a^2} + \frac{y_P^2}{b^2} + \frac{z_P^2}{c^2} = 1 \tag{2.9}$$

where the subscript P denotes that it is in the reference frame centered at the center of the planet and whose principal axes are aligned with those of the planet. In addition, a, b, c are the lengths of the planets principal axes. This is illustrated in the figure below.

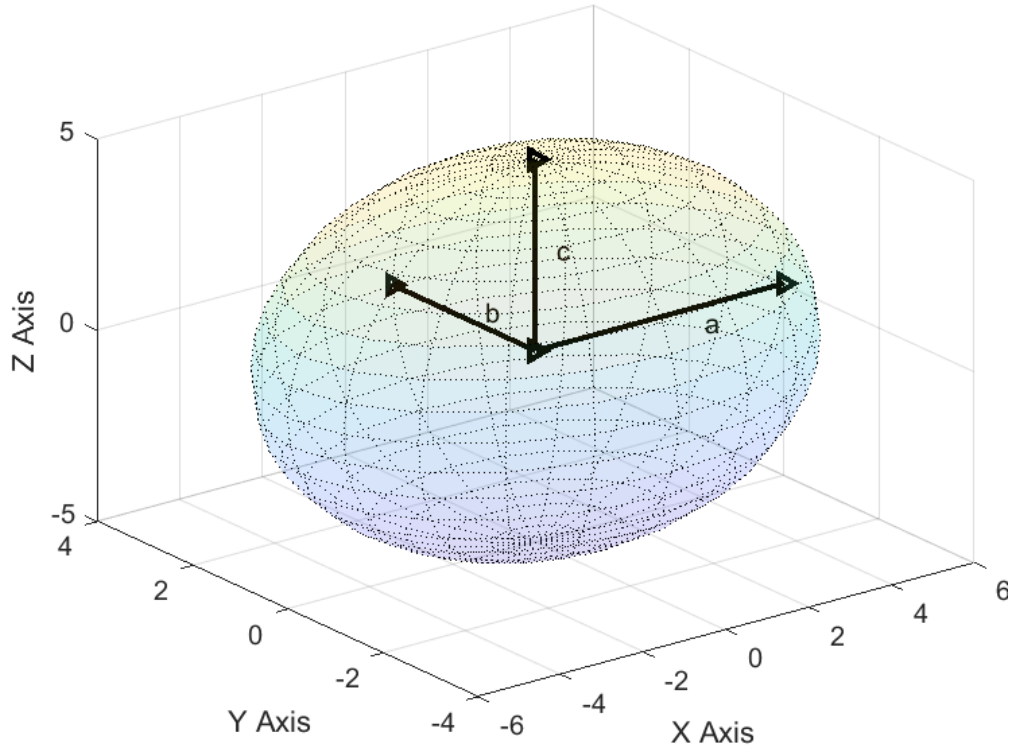

Figure 2.2: Visualization of a, b, and c

Therefore, the vector $\mathbf{p}_p^T = [x_P \quad y_P \quad z_P]$ is a point on the planets surface in the reference frame of the planets coordinate axes. Then, any point on the surface in the planet's fixed principal axes frame is constrained by

$$\mathbf{p}_P^T \begin{bmatrix} 1/a^2 & 0 & 0 \\ 0 & 1/b^2 & 0 \\ 0 & 0 & 1/c^2 \end{bmatrix} \mathbf{p}_P = \mathbf{p}_P^T \mathbf{A}_P \mathbf{p}_P = 1 \tag{2.10}$$

Due to the camera capturing the image, it is often more desirable to describe the planet shape in the frame of the camera's coordinate axes. Therefore, $\mathbf{T}_P^C$ is defined at the rotation matrix from the camera frame to the planet's principal axes frame. In practice, this rotation matrix is typically well known by combining spacecraft attitude information and planet ephemeris data. The spacecraft attitude can be calculated from sources such as on-board attitude filters using star trackers [17]. Therefore, rotating the planet surface vectors to the camera frame can be described by multiplying by the rotation matrix

$$\mathbf{p}_p = \mathbf{T}_P^C \mathbf{p}_C \tag{2.11}$$

substituting into Eq.(2.10),

$$\mathbf{p}_C^T \mathbf{T}_C^P \mathbf{A}_P \mathbf{T}_P^C \mathbf{p}_C = 1 \tag{2.12}$$

Then, following the frame rotation of matrices, the 3×3 symmetric, positive definite matrix, $\mathbf{A}_C$, describes the celestial body's shape in the camera's reference frame,

$$\mathbf{A}_C = \mathbf{T}_C^P \mathbf{A}_P \mathbf{T}_P^C \tag{2.13}$$

Combining the last two equations results in a completely rotated set of variables.

$$\mathbf{p}_C^T \mathbf{T}_C^P \mathbf{A}_P \mathbf{T}_P^C \mathbf{p}_C = \mathbf{p}_C^T \mathbf{A}_C \mathbf{p}_C = 1 \tag{2.14}$$

2.4.1 Derivation Using Geometry

The work that follows will be that of Dr. Christian [37]. Dr. Christian uses a geometric approach to form a quadratic in terms of the distance along a line of sight vector. With that, the equation for the ellipsoids tightly bounding cone is derived. Begin by recalling the planet model in the last equation.

With this model, the captured points in the picture belonging to the lit surface also lie along the rays that originate at the camera center and form a tangent to the surface of the planet or moon [37]. This complete set of rays forms a cone that tightly bounds the celestial body and creates an ellipse on the focal plane of the camera. A simple visualization, using aligned axis, for one set of vectors describing a point on the planets surface can be seen in the figure below, where $\mathbf{r}$ is the position of the camera relative to the center of the observed

celestial body.

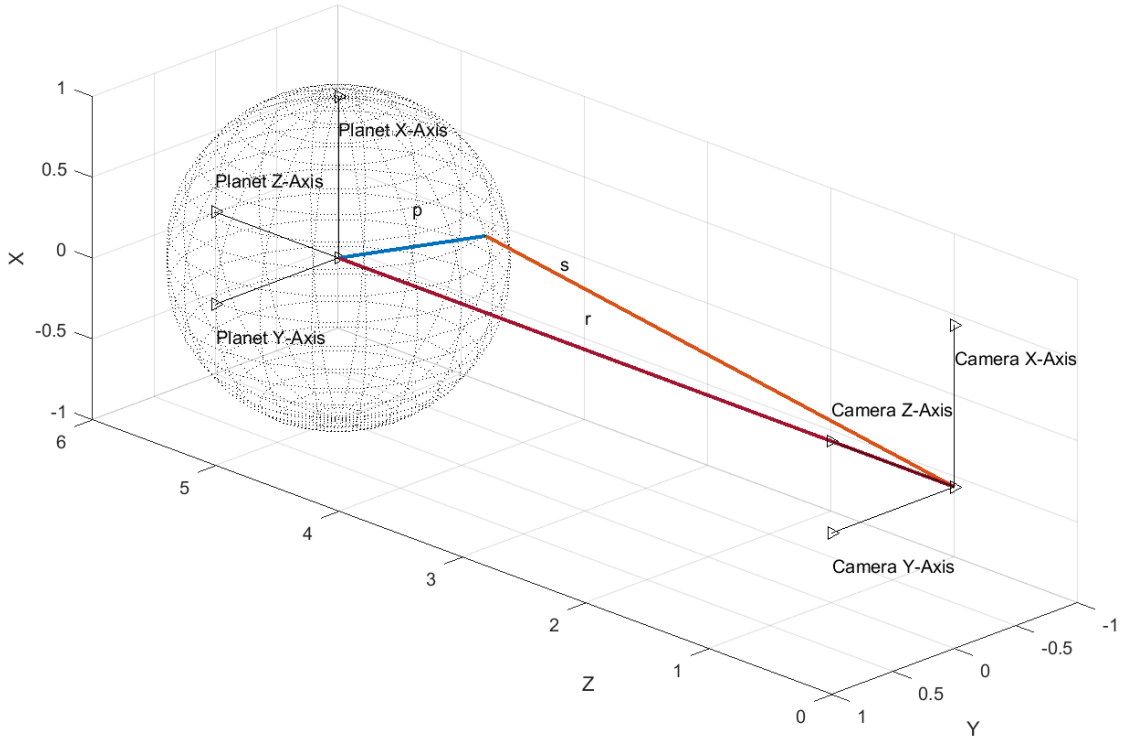

Figure 2.3: Visualization of Surface Point Vectors

By observing the figure above, it is clear that the vector $\mathbf{s}_i$, originating at the origin of the camera frame and going to point $\mathbf{p}_i$ on the surface of the body, can be described by vector algebra.

$$\mathbf{s}_i = \mathbf{p}_i - \mathbf{r} \tag{2.15}$$

If the vector, $\mathbf{s}_i$, is decomposed into it's unit vector, $\mathbf{e}_i$, and the distance along the vector before it intersects the surface of the planet, t, then the previous equation can be rearranged to a more advantageous format,

$$\mathbf{s}_i = \mathbf{p}_i - \mathbf{r} = t\mathbf{e}_i \tag{2.16}$$

$$\mathbf{p}_i = t\mathbf{e}_i + \mathbf{r} \tag{2.17}$$

substituting into Eq.(2.14),

$$(t\mathbf{e}_i + \mathbf{r})^T \mathbf{A}_C (t\mathbf{e}_i + \mathbf{r}) = 1 \tag{2.18}$$

Using the fact that $\mathbf{A}$ is symmetric and by moving the 1 to the left side, this can be expressed as a quadratic in terms of t,

$$(\mathbf{e}_i^T \mathbf{A} \mathbf{e}_i)t^2 + 2(\mathbf{e}_i^T \mathbf{A}\mathbf{r})t + (\mathbf{r}^T \mathbf{A}\mathbf{r} - 1) = 0 \tag{2.19}$$

Recall that the rays emanating from the center of the camera frame lie exactly tangent to the surface of the observed body. Therefore, the rays only intersect the body once and the value for t must have one repeated real root. If the vector $\mathbf{s}_i$ did not point to the horizon, it would intersect the planet twice, or not at all, and present a t with two roots. If the vector were to miss the planet completely, it would have two complex conjugate roots, and if it were to intersect the planet without being tangent to it, it would have two different real roots. In order to find the horizon points, one must find the solution in which the discriminant is equal to zero,

$$4(\mathbf{e}_i^T \mathbf{A}\mathbf{r})^2 - 4(\mathbf{e}_i^T \mathbf{A} \mathbf{e}_i)(\mathbf{r}^T \mathbf{A}\mathbf{r} - 1) = 0 \tag{2.20}$$

This scalar equation, quadratic in $\mathbf{e}_i$ can then be expanded to

$$\mathbf{e}_i^T [(\mathbf{A}\mathbf{r}\mathbf{r}^T \mathbf{A}) - (\mathbf{r}^T \mathbf{A}\mathbf{r} - 1)\mathbf{A}]\mathbf{e}_i = 0 \tag{2.21}$$

Since the above equation is equal to zero, it can be multiplied by t^2 in order to convert from the unit vector back to the vector to the surface of the planet and achieve the same results. Finally, the equation for the 3x3 symmetric matrix $\mathbf{M}$ may also be pulled from that,

$$\mathbf{s}_i^T[(\mathbf{A}\mathbf{r}\mathbf{r}^T\mathbf{A}) - (\mathbf{r}^T\mathbf{A}\mathbf{r} - 1)\mathbf{A}]\mathbf{s}_i = 0 \tag{2.22}$$

$$\mathbf{M} = ((\mathbf{A}\mathbf{r}\mathbf{r}^T\mathbf{A}) - (\mathbf{r}^T\mathbf{A}\mathbf{r} - 1)\mathbf{A}) \tag{2.23}$$

$$\mathbf{s}_i^T\mathbf{M}\mathbf{s}_i = 0 \tag{2.24}$$

This surface, formed by all possible values of $\mathbf{s}_i$, forms a cone that is identical to the one found earlier using the ellipse fit up to an unknown scalar value. Fortunately, this scalar value must not be solved for thanks to relatively recent work by Dr. Christian [41]. This equation for $\mathbf{M}$ presents an alternative method for extracting the values of $\mathbf{s}_i$ and can be used to eliminate the error associated with using an ellipse fit.

When working in focal length normalized coordinates, each $\mathbf{s}_i$ may be described by taking a sliced of the cone at $Z = 1$. This vector scaled by Z, $\hat{\mathbf{s}}_i$, is written as

$$\hat{\mathbf{s}}_i = \begin{bmatrix} x_i \\ y_i \\ 1 \end{bmatrix} \tag{2.25}$$

and can be substituted into Eq.(2.24). Due to Eq.(2.24) being equal to zero, $\mathbf{s}_i$ or $\hat{\mathbf{s}}_i$ can be used since the later is just a scaled version of the first. This scaling does not effect the equality of zero or, therefore, the final result. Plugging this into Eq.(2.24) yields an implicit quadratic equation where m_{jk} describes the $\{j, k\}$th element in the conic matrix $\mathbf{M}$,

$$m_{11}x_i^2 + 2m_{12}x_iy_i + 2m_{13}x_i + m_{22}y_i^2 + 2m_{23}y_i + m_{33} = 0 \tag{2.26}$$

Finally, by computing $\mathbf{M}$ and evaluating Eq.(2.26), the x_i and y_i values for each ray that originates at the camera center and is tangent to the surface of the observed body can be found [19].

2.4.2 Derivation Using Quadrics

Presented here is an alternative to the state of the art through the use of quadrics. The work that follows will be that of Hartley and Zisserman [33]. Instead of a quadratic approach, the use of quadrics is employed. The quadric describing the shape of the body is obtained, and with that the equation for the ellipsoids tightly bounding cone is derived. Begin by recalling the equation for an ellipsoid from before,

$$\mathbf{p}_P^T \mathbf{A}_C \mathbf{p}_P = 1 \tag{2.27}$$

Here, $\mathbf{p}$ is the vector from the center of the planet to a point on its surface and $\mathbf{A}$ is the planet's body shape matrix in the frame of the camera. Then, the above equation can be put into the quadric form,

$$\begin{bmatrix} \mathbf{p}^T & 1 \end{bmatrix} \begin{bmatrix} \mathbf{A} & \mathbf{0}_{3\times 1} \\ \mathbf{0}_{1\times 3}^T & -1 \end{bmatrix} \begin{bmatrix} \mathbf{p} \\ 1 \end{bmatrix} = \begin{bmatrix} X_i & Y_i & Z_i & 1 \end{bmatrix} \begin{bmatrix} 1/a^2 & 0 & 0 & 0 \\ 0 & 1/b^2 & 0 & 0 \\ 0 & 0 & 1/c^2 & 0 \\ 0 & 0 & 0 & -1 \end{bmatrix} \begin{bmatrix} X_i \\ Y_i \\ Z_i \\ 1 \end{bmatrix} = 0 \tag{2.28}$$

Recalling that $\mathbf{p}_P = \mathbf{s}_i - \mathbf{r}$ from vector decomposition, the equation above can be rewritten in terms of $\mathbf{s}_i$ and $\mathbf{r}$, which are both in the camera frame,

$$\begin{bmatrix} (\mathbf{s}_i - \mathbf{r})^T & 1 \end{bmatrix} \begin{bmatrix} \mathbf{A} & \mathbf{0}_{3\times 1} \\ \mathbf{0}_{1\times 3}^T & -1 \end{bmatrix} \begin{bmatrix} (\mathbf{s}_i - \mathbf{r}) \\ 1 \end{bmatrix} = 0 \tag{2.29}$$

Now that everything is in terms of the camera's frame, the inner matrix can be expanded to

$$\begin{bmatrix} \mathbf{s}_i^T & 1 \end{bmatrix} \begin{bmatrix} \mathbf{A} & -\mathbf{A}\mathbf{r} \\ -\mathbf{r}^T\mathbf{A}^T & \mathbf{r}^T\mathbf{A}\mathbf{r} - 1 \end{bmatrix} \begin{bmatrix} \mathbf{s}_i \\ 1 \end{bmatrix} = 0 \tag{2.30}$$

Therefore, the quadric for the observed celestial body can be defined as $\mathbf{Q}$,

$$\mathbf{Q} = \begin{bmatrix} \mathbf{A} & -\mathbf{Ar} \\ -\mathbf{r}^T\mathbf{A}^T & \mathbf{r}^T\mathbf{Ar} - 1 \end{bmatrix} \tag{2.31}$$

which matches the format according to Hartley's and Zisserman's [33] definition of the symmetric quadric $\mathbf{Q}$.

$$\mathbf{Q} = \begin{bmatrix} \mathbf{Q}_{3\times3} & \mathbf{q} \\ \mathbf{q}^T & q_{44} \end{bmatrix} \tag{2.32}$$

Therefore, one can relate similar variables,

$$\mathbf{Q}_{3\times3} = \mathbf{A} \tag{2.33}$$

$$\mathbf{q} = -\mathbf{Ar} \tag{2.34}$$

$$q_{44} = \mathbf{r}^T\mathbf{Ar} - 1 \tag{2.35}$$

This quadric can then be applied to determine the equation for the cone of rays that emanate from the camera center and tightly bound the observed quadric. This matrix describing the cone, $\mathbf{Q}_{co}$, is a degenerate quadric of rank 3 [33], this will be proved here shortly. Following Hartley and Zisserman [33], the equation for the conic surface is defined as,

$$\mathbf{Q}_{co} = (\mathbf{V}^T\mathbf{QV})\mathbf{Q} - (\mathbf{QV})(\mathbf{QV})^T \tag{2.36}$$

where $\mathbf{V}$ is the vertex of the cone of rays, and $\mathbf{Q}_{co}\mathbf{V} = 0$. Since all variables were previously rotated to the camera frame, the cone of rays originate at the center of the camera frame, placing the vertex of the cone at $\mathbf{V} = [0 \quad 0 \quad 0 \quad 1]^T$. Plugging this into Eq.(2.36) presents

the solution for the degenerate quadric $\mathbf{Q}_{co}$ as,

$$\mathbf{Q}_{co} = \begin{bmatrix} q_{44}\mathbf{Q}_{3\times3} - \mathbf{q}\mathbf{q}^T & \mathbf{0}_{3\times1} \\ \mathbf{0}_{1\times3} & 0 \end{bmatrix} \tag{2.37}$$

$\mathbf{Q}_{co}$ is clearly a degenerate matrix of rank three. Therefore, the upper 3×3 can be taken as the definition of $\mathbf{Q}_{co}$, satisfying the requirement that it lies tangent to the surface of the observed body,

$$\mathbf{s}_i^T(q_{44}\mathbf{Q}_{3\times3} - \mathbf{q}\mathbf{q}^T)\mathbf{s}_i = 0 \tag{2.38}$$

$$(q_{44}\mathbf{Q}_{3\times3} - \mathbf{q}\mathbf{q}^T) = (\mathbf{r}^T\mathbf{A}\mathbf{r} - 1)\mathbf{A} - \mathbf{A}\mathbf{r}\mathbf{r}^T\mathbf{A}^T \tag{2.39}$$

Since the right side of Eq.(2.38) is equal to zero, it can be multiplied by any scaling factor and still define the same quadric. Therefore, Eq.(2.39) can be scaled by a factor of -1 to arrive at the same solution as in the previous section [18].

$$\mathbf{M} = \mathbf{A}\mathbf{r}\mathbf{r}^T\mathbf{A}^T - (\mathbf{r}^T\mathbf{A}\mathbf{r} - 1)\mathbf{A} \tag{2.40}$$

As can be seen, both methods present the exact same solution for the bounding cone $\mathbf{M}$. After calculating the conic shape matrix, $\mathbf{M}$, the same method as earlier can be applied to solve for $\mathbf{s}_i$. Therefore, a method of using quadrics to determine the equation of the tightly bounding cone has been presented through the use of single view geometry. Both methods show potential in all OPNAV scenarios where the relative frame rotation between the camera and the planets principal axis is known.

By using either method to calculate $\mathbf{M}$ and then the values of $\mathbf{s}_i$, the derivation may continue to find the relative distance from the camera center to the center of the principal axis of the observed celestial body.

2.5 Position Determination from Body of Known Orientation

After using either method to derive $\mathbf{M}$ and the values of $\mathbf{s}_i$, the procedure for finding the relative position of the spacecraft from the planets principal axis makes use of matrix factorization to solve the problem without iteration. The following result is the spacecraft's position that creates the horizon ellipse that best fits the surface of the observed ellipsoid. The algorithm is presented here with analytical proof in Chapter 4.

Begin by factorizing the body shape matrix $\mathbf{A}$. This is a reasonable equation to use because the matrix $\mathbf{A}$ is positive-definite and symmetric. There are multiple ways to factorize the matrix, however this specific choice is well proven by Dr. John Christian [41]. Once again, the work that follows in this chapter is entirely his work.

$$\mathbf{A} = \mathbf{B}^T\mathbf{B} \tag{2.41}$$

In order to arrive at an analytical solution, through the use of matrix factorization, singular value decomposition (SVD) can be performed to produce a simple solution for the relative distance vector, $\mathbf{r}$. Although the solution may be arrived at by using Cholesky decomposition [18], the SVD approach can be expressed in a straightforward procedure. Therefore, assume the body shape matrix $\mathbf{A}$ is factorized by SVD,

$$\mathbf{A} = \mathbf{U}\mathbf{S}\mathbf{V}^T \tag{2.42}$$

In SVD, the $\mathbf{U}$ and $\mathbf{V}$ are orthogonal matrices and $\mathbf{S}$ is a diagonal matrix containing singular values. Due to $\mathbf{A}$ being a real-valued symmetric matrix, $\mathbf{U} = \mathbf{V}$ and the values in $\mathbf{S}$ must be non-zero. It can be seen that the SVD matches the same form as in Eq.(2.13), therefore the values of $\mathbf{U}$, $\mathbf{S}$, and $\mathbf{V}$ do not need to actually be solved through SVD. Substituting the values from Eq.(2.13) leads to

$$\mathbf{U} = \mathbf{V} = \mathbf{T}_C^P \qquad \mathbf{U}^T = \mathbf{V}^T = \mathbf{T}_P^C \tag{2.43}$$

$$\mathbf{S} = \mathbf{A}_p = \begin{bmatrix} 1/a^2 & 0 & 0 \\ 0 & 1/b^2 & 0 \\ 0 & 0 & 1/c^2 \end{bmatrix} \tag{2.44}$$

Recall that a, b, c are the principal axes dimensions of the triaxial ellipsoid, therefore they must be greater than zero. Then, the same factorization from before applied to the matrix $\mathbf{S}$ presents

$$\mathbf{S} = \mathbf{A}_P = \mathbf{Q}^T\mathbf{Q} \tag{2.45}$$

$$\mathbf{Q} = \begin{bmatrix} 1/a & 0 & 0 \\ 0 & 1/b & 0 \\ 0 & 0 & 1/c \end{bmatrix} \tag{2.46}$$

These values can then be substituted back into the SVD equation and the original factorization. Taking note of the orthogonality condition of rotation matrices that $\mathbf{T}_P^C\mathbf{T}_C^P = \mathbf{I}$ [42], a numerical value can be found for $\mathbf{B}$ through

$$\mathbf{A} = \mathbf{B}^T\mathbf{B} = \mathbf{T}_C^P\mathbf{Q}^T\mathbf{Q}\mathbf{T}_P^C \tag{2.47}$$

$$\mathbf{B} = \mathbf{Q}\mathbf{T}_P^C \tag{2.48}$$

From here, the factorized matrix $\mathbf{B}$, may be used. The matrix $\mathbf{B}$ can be used to transform the $\mathbf{s}_i$ line of sight vectors to the surface of the celestial body into a new factorized space, following

$$\bar{\mathbf{s_i}} = \mathbf{B}\mathbf{s}_i \tag{2.49}$$

Then, the unit vector must be found for $\bar{\mathbf{s_i}}$ in the factorized space [18] by using

$$\bar{\mathbf{s_i}}' = \frac{\bar{\mathbf{s_i}}}{||\bar{\mathbf{s_i}}||} \tag{2.50}$$

From here, the solution can be found by using a least-squares. After assembling values of $\bar{\mathbf{s_i}}$ into a $3 \times m$ matrix and solving for the value of $\mathbf{n}$, following

$$\begin{bmatrix} \bar{\mathbf{s_1}}'^T \\ \bar{\mathbf{s_2}}'^T \\ \cdots \\ \bar{\mathbf{s_m}}'^T \end{bmatrix} \mathbf{n} = \mathbf{1}_{m \times 1} \tag{2.51}$$

a simple estimate for the camera location $\mathbf{r}$ is given by

$$\mathbf{Br} = -(\mathbf{n}^T\mathbf{n} - 1)^{-1/2}\mathbf{n} \tag{2.52}$$

Since $\mathbf{B}$ is simply a modified body shape matrix multiplied by the rotation matrix, which are both invertible and well known, the final solution for $\mathbf{r}$ may be written by inverting $\mathbf{B}$ and moving it to the right side. This can be directly written as

$$\mathbf{r} = -(\mathbf{n}^T\mathbf{n} - 1)^{-1/2}\mathbf{T}_C^P\mathbf{Q}^{-1}\mathbf{n} \tag{2.53}$$

The solution here provides an exact solution, depending on the method of procuring $\mathbf{s}_i$, and only uses the two assumptions that the body is a smooth triaxial ellipsoid and that a pinhole camera model is accurate for image projection representation.

3. Attitude Determination of Chaotically Rotating Body

3.1 Camera Attitude Estimation

The previously presented methods are proven accurate for most practical applications of OPNAV. However, the baseline requirement for those calculations is that the ephemeris data is available for the observed celestial body. It is clear that there is a need for OPNAV techniques that apply to bodies in which this information is not available, primarily bodies in a chaotic rotation state. In typical OPNAV scenarios, the relative rotation of the planet is known and the distance is the uknown to be solved. The method presented here takes a different approach. Assuming that the relative distance between the spacecraft and planet is known, the attitude of the celestial body relative to the spacecraft can be obtained up to a two fold ambiguity. Since the attitude of the spacecraft relative to Earth is usually known, the orientation of the body with unknown attitude can also be related to Earth's axes. The method presented here offers an application for solving the attitude of any of these chaotically rotating bodies relative to an observing spacecraft. Following identical procedures as found by Christian [43] and Modenini [44], the solution can be found in the form of a modified Procrustes problem. Modenini takes advantage of variables that may not be known in OPNAV, therefore, some of Dr. Chirtian's work [43] is used to form a different basis for the similar procedure found in Modenini's work. However, this methodology is entirely new and a combination of similar techniques.

Utilizing the same assumptions from the previous chapter, it is without a loss of generality that the triaxial ellipsoid planet be considered centered in the origin of the planet frame with the axes aligned to those of the planets principal axes. In practice, the dimensions of the ellipsoid should be well known from a combination of other OPNAV techniques and Earth measurements. Thus, the 4×4 symmetric matrix, $\mathbf{Q_p}$, describes the shape of the body with respect to the body's center in homogeneous coordinates,

$$\mathbf{Q_P} = \begin{bmatrix} a^2 & 0 & 0 & 0 \\ 0 & b^2 & 0 & 0 \\ 0 & 0 & c^2 & 0 \\ 0 & 0 & 0 & -1 \end{bmatrix} \tag{3.1}$$

Where, like before, $\{a, b, c\}$ are the lengths of the body's principal axes. It is clear that the orientation of the bodies principal axes relative to the spacecraft is necessary for all non-spherical bodies.

Now, suppose that a spacecraft equipped with a calibrated camera [45] is located at distance $\mathbf{r}$, relative to the center of the celestial body. It is a reasonable assumption that $\mathbf{r}$ is known from the distance at which lit limb OPNAV occurs. This relative distance may be found using a rangefinder or through the use of deep space network tracking. Now, introduce $\mathbf{P}$, which is the camera calibration matrix from the planets fixed principal axes to the camera frame. Now, $\mathbf{T}_c^p$ will be used to represent the rotation matrix between the camera frame axes and the principal axes of the observed body. All subsequent analyses will rely on the following known transformation from perspective geometry [33],

$$\mathbf{P}_c^p = \mathbf{T}_c^p[I \quad \mathbf{r}_p] \tag{3.2}$$

The quadric $\mathbf{Q}_p^{-1}$ transforms to the conic $\mathbf{C}$ on the image plane, and can be described in the camera frame by multiplying by the camera calibration matrix,

$$\mathbf{C}^{-1} \propto \mathbf{P}_c^p \mathbf{Q}_p^{-1} \mathbf{P}_p^c \tag{3.3}$$

Eq.(3.3) is reasonable up to a constant factor because the symmetric matrix $\mathbf{C}$ represents the conic in homogeneous coordinates and is fully determined [44]. Therefore, it can be rewritten as an equality by introducing the scaling factor α such that

$$\alpha \mathbf{C}^{-1} = \mathbf{P}_c^p \mathbf{Q}_p^{-1} \mathbf{P}_p^c \tag{3.4}$$

Here, α is an unknown constant to be determined and $\mathbf{C}$ is computed from the previously mentioned ellipse quadratic. Where the $\mathbf{C}$ here is the same presented through an ellipse fit mentioned earlier using the pinhole camera model. Later, it will become necessary to use the assumption from before that the focal length $f = 1$ in order to work in focal length normalized coordinates.

Then, $\mathbf{A}_p^{-1}$ can be defined as the 3×3 matrix describing the body shape of the observed planet since the quadratic matrix $\mathbf{Q}_p^{-1}$ admits the following block diagonal decomposition,

$$\mathbf{Q}_p^{-1} = \begin{bmatrix} \mathbf{A}_p^{-1} & 0 \\ 0 & -1 \end{bmatrix} \tag{3.5}$$

Noting Eq.(3.2) and Eq.(3.5), the rotational and translational parts of the transformation in Eq.(3.4) can be decoupled according to the following

$$\alpha \mathbf{C}^{-1} = \mathbf{T}_c^p (\mathbf{A}_p^{-1} - \mathbf{r_p} \mathbf{r_p}^T) \mathbf{T}_p^c \tag{3.6}$$

Following matrix algebra, this can be expanded to

$$\alpha \mathbf{C}^{-1} = \mathbf{T}_c^p \mathbf{A}_p^{-1} \mathbf{T}_p^c - \mathbf{T}_c^p \mathbf{r_p} \mathbf{r_p}^T \mathbf{T}_p^c \tag{3.7}$$

Since $\mathbf{r}_p$, the distance from the center of the planet to the camera center in the coordinate frame of the planet, is most likely unknown, it will be converted into the known $\mathbf{r}_c$ by multiplying by the rotation matrix.

$$\mathbf{r}_C = \mathbf{T}_c^p \mathbf{r}_p \tag{3.8}$$

Therefore, Eq.(3.7) can be written in the solvable form by replacing the distance vectors. This results in,

$$\alpha \mathbf{C}^{-1} = \mathbf{T}_c^p \mathbf{A}_p^{-1} \mathbf{T}_p^c - \mathbf{r}_C \mathbf{r}_C^T \tag{3.9}$$

3.2 Solving for the Rotation Matrix

Given Eq.(3.9), it can be seen that there are similar matrices on both sides of the equation. The determination of the scaling factor α is found by taking the trace of the equation,

$$\alpha tr[\mathbf{C}^{-1}] = tr[\mathbf{T}_c^p \mathbf{A}_p^{-1} \mathbf{T}_p^c - \mathbf{r}_C \mathbf{r}_C^T] \tag{3.10}$$

$$\alpha tr[\mathbf{C}^{-1}] = tr[\mathbf{T}_c^p \mathbf{A}_p^{-1} \mathbf{T}_p^c] - tr[\mathbf{r}_C \mathbf{r}_C^T] \tag{3.11}$$

Note that because of the fact that the rotation matrix is an orthogonal matrix, the trace of the rotated body shape matrix is the same as the trace of the original matrix such that

$$tr[\mathbf{T}_c^p \mathbf{A}_p^{-1} \mathbf{T}_p^c] = tr[\mathbf{A}_p^{-1}] \tag{3.12}$$

Eq.(3.11) can be rewritten by plugging in the above equation. Resulting in

$$\alpha tr[\mathbf{C}^{-1}] = tr[\mathbf{A}_p^{-1}] - tr[\mathbf{r}_C \mathbf{r}_C^T] \tag{3.13}$$

Then, α can be solved for through linear algebra such that

$$\alpha = \frac{tr[\mathbf{A}_p^{-1}] - tr[\mathbf{r}_C \mathbf{r}_C^T]}{tr[\mathbf{C}^{-1}]} \tag{3.14}$$

Therefore, the inverse projected ellipse matrix is scaled by α, which depends on the principal axes lengths of the projected ellipsoid and the position of the observing spacecraft. Using the above equation, the exact numerical value can be found for α.

To solve for the rotation matrix $\mathbf{T}$, the distance vectors can be moved to the other side of the equal sign in Eq.(3.9) according to

$$\mathbf{T}_C^P \mathbf{A}_P^{-1} \mathbf{T}_P^C = \alpha \mathbf{C}^{-1} + \mathbf{r}_C \mathbf{r}_C^T \tag{3.15}$$

This can then be rearranged to fit the well known orthogonal Procrustes format by multiplying the right sides by the inverse rotation matrix. This modified orthogonal Procrustes presents the rotation matrix solution to Wahba's problem [46] which used multiple vector observations [47]. This presents the similar transformation,

$$\mathbf{T}_C^P \mathbf{A}_P^{-1} = (\alpha \mathbf{C}^{-1} + \mathbf{r}_C \mathbf{r}_C^T) \mathbf{T}_C^P \tag{3.16}$$

Now, a modified orthogonal Procrustes approach can be taken through spectral decomposition. Given two symmetric matrices $\boldsymbol{A}$ and $\boldsymbol{B}$, the following decomposition can be performed

$$\mathbf{A} = (\alpha \mathbf{C}^{-1} + \mathbf{r}_C \mathbf{r}_C^T) = \mathbf{U} \mathbf{D}_A \mathbf{U}^T \tag{3.17}$$

$$\mathbf{B} = \mathbf{A}_P^{-1} = \mathbf{V} \mathbf{D}_B \mathbf{V}^T \tag{3.18}$$

Then, the solution to the orthogonal matrix which maps the points in $\boldsymbol{A}$ to the closest corresponding points in $\boldsymbol{B}$ is satisfied by the Frobenius norm minimization

$$\begin{aligned} &\min_T \|\mathbf{AT} - \mathbf{TB}\|_F^2 \\ &subject\ to\ \mathbf{T}^T \mathbf{T} = \mathbf{I} \end{aligned} \tag{3.19}$$

Therefore, the solution is given by any matrix of the form

$$\mathbf{T}_C^P = \mathbf{UPV}^T \tag{3.20}$$

where $\mathbf{P} = diag\{\pm 1 \pm 1 \pm 1\}$. All eight possible solutions given by Eq.(3.20) provide the same residual Frobenius norms, however, the current interest is only in those that generate proper rotation matrices [44]. Proper rotation matrices can be found where the $\det(\mathbf{T}) = 1$. If it is assumed that the $\det(\mathbf{UV^T}) = 1$, the possibilities of $\mathbf{P}$ are reduced to four options in order to achieve a proper rotation matrix. The four options are matrices in which the $\det(\mathbf{P}) = 1$, presenting the solutions of

$$diag(\mathbf{P}) = \begin{cases} [+1, +1, +1] \\ [-1, -1, +1] \\ [+1, -1, -1] \\ [-1, +1, -1] \end{cases} \tag{3.21}$$

Therefore, there is a four fold ambiguity in the current solution. However, this can be further reduced to two options by examining the sign of the Z component. Out of these options, only two of them correspond to the ellipsoid being down the boresight of the camera. Following the pinhole camera method, the Z-axis is along the camera boresight and is positive out of the camera [41] such that any vector from the camera to the planet's center, $\mathbf{r}$, with a positive Z component, will depict the camera facing the observed body.

Then, due to the natural symmetry of triaxial ellipsoids, the solution method presents a twofold equivocacy in the rotation matrix. This is easy to visualize in the figure below when considering a camera pointing at the body because they may differ by a 180 degree rotation about the optical axis.

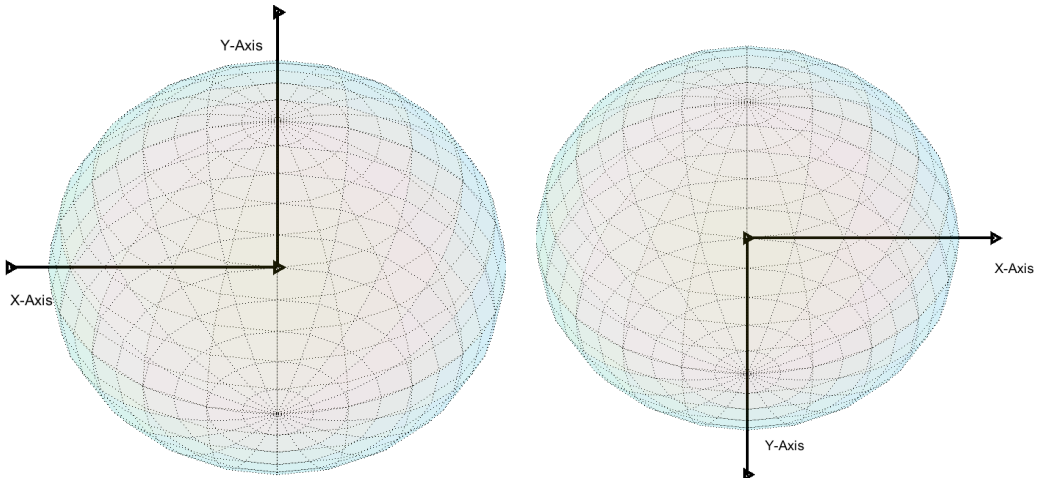

Figure 3.1: Demonstration of Indistinguishable Attitudes

In order to determine the correct solution, more information is required such as recent attitude history or information from other sensors. In addition, the use of surface features could be utilized to better determine the exact orientation with the assistance of this method.

Therefore, a new solution to attitude estimation for chaotically rotating, or tumbling bodies without a stable axis of rotation has been presented. Unlike the usual situation of knowing the relative rotation and solving for distance, this method assumes that the relative distance is known and calculates the relative rotation from the body's principal axes to the spacecraft's. Through the use of an ellipse fit on the image of a celestial body and perspective geometry, the rotation matrix is computed by solving a modified orthogonal Procrustes problem. The optimal solution, given by a Frobenius norm minimization, presents a solution of two symmetric matrices. Further work is required to improve the results, including error analysis under real-world scenarios along with a further look into methods to reduce the two-fold ambiguity. In addition, the ellipse fit technique presents a small amount of error that should be reduced. Further work should include attempting to apply another method of extracting the conic, such as using quadrics.

4. Numerical Results

4.1 Simulation Setup

Two different calculations will be performed here. The first will demonstrate that an exact solution for the relative distance to an observed body from a spacecraft can be obtained through a moons lit limb. The second example will demonstrate that a two fold ambiguous solution for the relative rotation of an unknown body can be solved by starting with a known distance. For these examples, due to the lack of actual data, a simulation will be used to demonstrate the ability of both OPNAV techniques. For these examples, the shape of the body will match that of Saturn's moon Hyperion, which has principal axes lengths of $[410 \quad 260 \quad 220]km$. For these examples, an arbitrary distance vector, $\mathbf{r}$, and rotation matrix, $\mathbf{R}$, were also selected. The same variables will be used for both methods to demonstrate similarities.

4.2 Using Known Attitude to Obtain Position

The first section will start by assuming that the relative rotation matrix is known. Following the method outlined earlier, the relative distance vector will be computed and compared to the input value. Start by examining the inputs to the simulation. An arbitrary distance vector $\mathbf{r}$ was chosen and the principal axis of Hyperion were used to define the body describing matrix $\mathbf{A}_P$,

$$\mathbf{r} = \begin{bmatrix} 500 \\ 600 \\ 700 \end{bmatrix} \quad \mathbf{A}_P = \begin{bmatrix} 1/410^2 & 0 & 0 \\ 0 & 1/260^2 & 0 \\ 0 & 0 & 1/220^2 \end{bmatrix} \tag{4.1}$$

Then, the rotation matrix $\mathbf{R}$ was calculated from a random rotation vector $\mathbf{k}$ and angle of

rotation θ. This rotation matrix is assumed to be known for the rest of the calculations in this section. This will also be the rotation matrix to be solved for in the next section.

$$\mathbf{R} = \mathbf{I} - sin(\theta)\mathbf{k}^{\times} + (1 - cos(\theta)\mathbf{k}^{\times}\mathbf{k}^{\times} \tag{4.2}$$

$$\mathbf{R} = \begin{bmatrix} -0.6768 & -0.5117 & 0.5292 \\ 0.5755 & 0.0806 & 0.8138 \\ -0.4591 & 0.8554 & 0.2399 \end{bmatrix} \tag{4.3}$$

This was then used to model the body in space relative to a camera at the origin. A representation of the 3D view and plotted ellipse fit can be seen below where the red line in the image is the ellipse projected on the image from the planet.

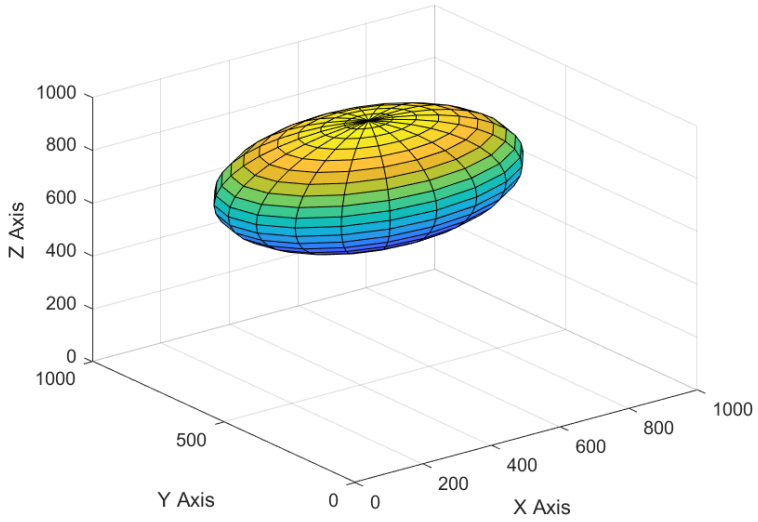

Figure 4.1: Simulated 3D View

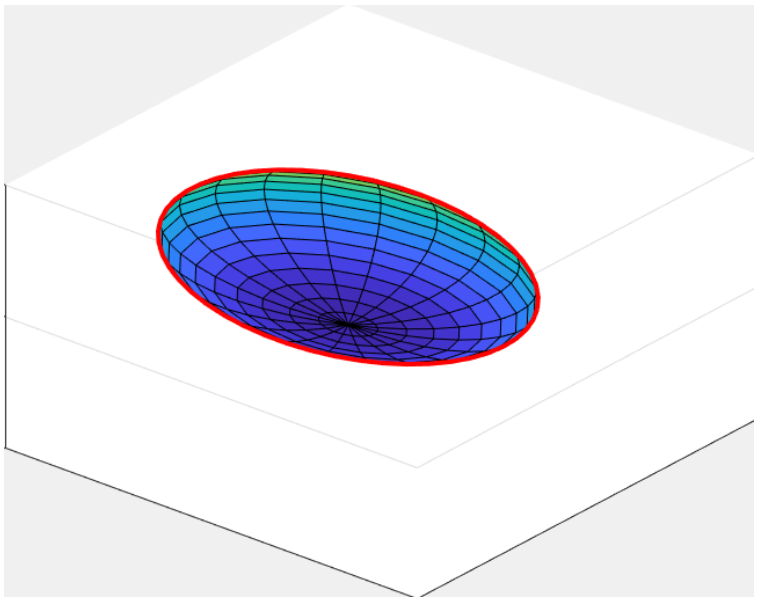

Figure 4.2: Ellipse Projected on Focal Plane

Then, the equation of the set of tightly bounding arrays can be obtained using Eq(2.40).

$$\mathbf{M} = \begin{bmatrix} -0.1698 & 0.0089 & 0.1257 \\ 0.0089 & -0.0839 & 0.0869 \\ 0.1257 & 0.0869 & -0.1494 \end{bmatrix} \times 10^{-3} \tag{4.4}$$

With the equation of the tightly bounding cone, the x and y starting points for each ray to the surface of the body were calculated. From that, the $\mathbf{s}_i$ vectors were extracted. With the $\mathbf{s}_i$ vectors, they were then translated into the factorized space. Begin by calculating the factorization matrix $\mathbf{B}$,

$$\mathbf{B} = \begin{bmatrix} 1/410 & 0 & 0 \\ 0 & 1/260 & 0 \\ 0 & 0 & 1/220 \end{bmatrix} \begin{bmatrix} -.677 & .576 & -.459 \\ -.512 & .081 & .855 \\ .529 & .814 & .239 \end{bmatrix} = \begin{bmatrix} -.0017 & .0014 & -.0011 \\ -.0020 & .0003 & .0033 \\ .0024 & .0037 & .0011 \end{bmatrix} \tag{4.5}$$

With the factorization matrix $\mathbf{B}$, the ray vectors can be put into a factorized space

and a least squares can be applied to solve for $\mathbf{n}$. These steps will not be included because they are straightforward. However, the calculated value of $\mathbf{n}$ can be found to be

$$\begin{bmatrix} \bar{s_1}'^T \\ \bar{s_2}'^T \\ \dots \\ \bar{s_m}'^T \end{bmatrix} \mathbf{n} = 1_{m\times 1} \tag{4.6}$$

$$\mathbf{n} = \begin{bmatrix} -0.174 \\ 0.341 \\ 0.950 \end{bmatrix} \tag{4.7}$$

Finally, the value for the distance vector can be calculated following Eq.(2.53) and compared to the $\mathbf{r}$ used to create the model.

$$\mathbf{r}_{Output} = \begin{bmatrix} 500 \\ 600 \\ 700 \end{bmatrix} \quad \mathbf{r}_{Input} = \begin{bmatrix} 500 \\ 600 \\ 700 \end{bmatrix} \tag{4.8}$$

As can be seen, the values are exactly the same. Therefore, the method presented offers a way to exactly obtain the distance vector from the camera to the planet assuming a known rotation matrix. In the following section, the same values will be used for creating the model, but the distance vector will assumed to be known and the rotation matrix will be assumed unknown.

4.3 Using Known Position to Obtain Attitude

The next section will start by assuming that the relative distance vector is known. Following the method outlined earlier, the two relative rotation matrices will be computed and compared to the input value. Start by examining the inputs to the simulation, which are the same as in the last example. An arbitrary distance vector $\mathbf{r}$ was chosen and the principal axis of Hyperion were used to define the body describing matrix $\mathbf{A}_P$. In addition,

the same rotation matrix is used here.

$$\mathbf{r} = \begin{bmatrix} 500 \\ 600 \\ 700 \end{bmatrix} \quad \mathbf{A}_P = \begin{bmatrix} 1/410^2 & 0 & 0 \\ 0 & 1/260^2 & 0 \\ 0 & 0 & 1/220^2 \end{bmatrix} \tag{4.9}$$

$$\mathbf{R} = \begin{bmatrix} -0.6768 & -0.5117 & 0.5292 \\ 0.5755 & 0.0806 & 0.8138 \\ -0.4591 & 0.8554 & 0.2399 \end{bmatrix} \tag{4.10}$$

Following the creation of the model, the same ellipse was projected to the image plane as in Fig(4.2). Then, an ellipse fit was applied to the projection to obtain $\mathbf{C}$ and converted from pixal coordinates. Then, with $\mathbf{C}^{-1}$, the traces can be used in Eq.(3.14) to calculate α as

$$\alpha = -19.37 \tag{4.11}$$

Then, with α, the SVD can be composed according to Eq.(3.17-3.19) to solve for $\mathbf{U}$ and $\mathbf{V}^T$.

$$\mathbf{U} = \begin{bmatrix} -0.6768 & 0.5117 & -0.5292 \\ 0.5755 & -0.0806 & -0.8138 \\ -0.4591 & -0.8554 & -0.2399 \end{bmatrix} \mathbf{V}^T = \begin{bmatrix} 1 & 0 & 0 \\ 0 & 1 & 0 \\ 0 & 0 & 1 \end{bmatrix} \tag{4.12}$$

It can be seen that the assumption made earlier that $det(\mathbf{U}\mathbf{V}^T) = 1$ is satisfied by these values. Then, the four possible values for the rotation matrix can be found using Eq.(3.20).

$$\mathbf{T}_1 = \begin{bmatrix} -0.6768 & 0.5117 & -0.5292 \\ 0.5755 & -0.0806 & -0.8138 \\ -0.4591 & -0.8554 & -0.2399 \end{bmatrix} \mathbf{T}_2 = \begin{bmatrix} 0.6768 & -0.5117 & -0.5292 \\ -0.5755 & 0.0806 & -0.8138 \\ 0.4591 & 0.8554 & -0.2399 \end{bmatrix} \tag{4.13}$$

$$\mathbf{T}_3 = \begin{bmatrix} -0.6768 & -0.5117 & 0.5292 \\ 0.5755 & 0.0806 & 0.8138 \\ -0.4591 & 0.8554 & 0.2399 \end{bmatrix} \mathbf{T}_4 = \begin{bmatrix} 0.6768 & 0.5117 & 0.5292 \\ -0.5755 & -0.0806 & 0.8138 \\ 0.4591 & -0.8554 & 0.2399 \end{bmatrix} \tag{4.14}$$

It can be observed that only two of these rotation matrices satisfy the requirement that **Tr** presents a positive value along the Z-axis, corresponding to the planet being along the boresight of the camera. The rotations that satisfy this requirement are $\mathbf{T}_2$ and $\mathbf{T}_3$. Therefore, a two fold ambiguity is left in the solution for the rotation matrix.

$$\mathbf{T}^P_{COutput} = \begin{bmatrix} 0.6768 & -0.5117 & -0.5292 \\ -0.5755 & 0.0806 & -0.8138 \\ 0.4591 & 0.8554 & -0.2399 \end{bmatrix} or \begin{bmatrix} -0.6768 & -0.5117 & 0.5292 \\ 0.5755 & 0.0806 & 0.8138 \\ -0.4591 & 0.8554 & 0.2399 \end{bmatrix} \tag{4.15}$$

$$\mathbf{T}^P_{CInput} = \begin{bmatrix} -0.6768 & -0.5117 & 0.5292 \\ 0.5755 & 0.0806 & 0.8138 \\ -0.4591 & 0.8554 & 0.2399 \end{bmatrix} \tag{4.16}$$

It can be seen that the correct solution for the rotation matrix is exactly one of the two possible solutions. However, in the figure below, the two possible solutions present the same solution for a projected ellipse on the image plane.

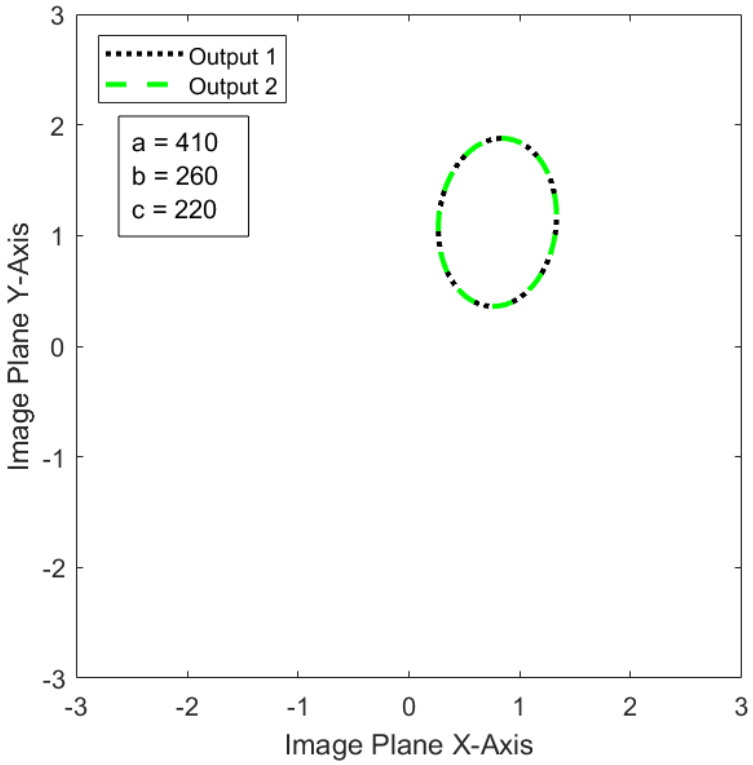

Figure 4.3: Projected Ellipse From Both Potential Solutions

Therefore, the ability to solve for the relative rotation of the planets principal axis to those of the spacecraft has been presented. Assuming that the distance from the spacecraft to the planet is known, a solution with two-fold ambiguity is obtained. The solution presented here happened to return the exact solution, however, it is assumed that is only because it is an ideal simulation. Due to the ellipse fit to get $\mathbf{C}$, the final solution would likely have more error. However, similar analysis have found that the mean error is typically on the order of 4 arcseconds [44].

5. Conclusion

This thesis presented a solution to orientation estimation for celestial bodies with unknown attitude. This problem is applicable for spacecraft attitude determination through the captured image of a triaxial ellipsoid. For typical OPNAV scenarios, the relative rotation of the planets principal axis to those of the spacecraft is known and the relative distance is to be computed, however, this thesis took the opposite approach. Through the use of an ellipse fit on the image of a celestial body and single view geometry, the rotation matrix is obtained. The optimal solution, given by a Frobenius norm minimization, presents a solution of two symmetric matrices.

To conclude, the presented attitude determination technique shows promise in future autonomous spacecraft navigation. With a known distance vector from a spacecraft to a planet of unknown orientation, it has been proven that the planets relative attitude can be obtained. Then, since the spacecraft's dynamics are typically known, the planets orientation relative to Earth can be obtained. Further work is required to improve the results including error analysis under real-world scenarios along with a further look into methods to reduce the two-fold ambiguity.

LITERATURE CITED

[1] B. Lampkin, "Sextant Sighting Performance for Space Navigation Using Simulated and Real Celestial Targets," *NAVIGATION,* vol. 12, no. 4, pp. 312–320, 1965, doi: 10.1002/navi.1965.12.issue-4.

[2] T. Jorris and A. Barth, "The USAF Manned Space Navigation Experiment on Apollo and Its Implications on Advanced Manned Spacecraft," in *Proc. Inst. Nav. Nat. Space Meeting,* Washington, D.C., 1968, pp. 219–240.

[3] D. Smith and B. Lampkin, "Sextant Sighting Measurements from on Board the Gemini XII Spacecraft," NASA, Moffett Field, CA, USA, NASA TN D-4952, Dec. 1968. Accessed: April 2020. [Online]. Available: https://ntrs.nasa.gov/api/citations/19690005000/downloads/19690005000.pdf

[4] W. Owen, T. Duxbury, C. Action, S. Synnott, J. Riedel, and S. Bhaskaran, "A Brief History of Optical Navigation at JPL," presented at the Amer. Astronautical Soc. Guid. Control Conf., Springfield, VA, USA, Feb., 2008. Amer. Astronautical Soc. Paper 08-053.

[5] T. Duxbury and W. Breckenridge, "Mariner Mars 1969 Optical Approach Navigation," in *8th Aerosp. Sci. Meet.,* 1970, doi: 10.2514/6.1970-70.

[6] W. Owen, "Methods of Optical Navigation," in *Proc. AAS/AIAA Space Flight Mechanics Meet.,* Springfield, VA, Feb. 2011. [Online]. Accessed May, 2020. Available: https://trs.jpl.nasa.gov/bitstream/handle/2014/41942/11-0589.pdf?sequence=1&isAllowed=y

[7] J. Campbell, S. Synnott, and G. Bierman, "Voyager Orbit Determination at Jupiter," *IEEE Trans. Autom. Control,* vol. 28, no. 3,pp. 256–268, 1983, doi: 10.1109/TAC.1983.1103223.

[8] J. Jordan and L. Wood, "Interplanetary Navigation: An Overview," in *Localization and Orientation in Biology and Engineering,* New York, NY, USA: Springer 1984, pp. 294–305. [Online]. Available: https://doi.org/10.1007/978-3-642-69308-3_53. Accessed: May, 2020.

[9] J. Christian and E. Lightsey, "Onboard Image-Processing Algorithm for a Spacecraft Optical Navigation Sensors System," *J. Spacecr. Rockets,* vol. 49, no. 2, pp. 337–352, 2012, doi: 10.2514/1.A32065

[10] J. Christian and C. Hollenberg, "Initial Orbit Determination from Three Velocity Vectors," *J Guid Control Dyn,* vol. 42, no. 4, pp. 894–899, 2019, doi: 10.2514/1.G003988.

[11] J. Christian and C. Hollenberg, "Geometric Solutions for Problems in Velocity-Based Orbit Determination," *J. Astronaut. Sci.,* vol. 67,pp. 188–224, 2020, doi: 10.1007/s40295-019-00170-7.

[12] N. Jerath and H. Ohtakay, "Mariner IX Optical Navigation Using Mars Lit Limb," *J. Spacecr. Rockets,* vol. 11, no. 7, pp. 505–511, 1974, doi: 10.2514/3.62114.

[13] Y. Cheng, A. Johnson, L. Matthies, and C. Olson, "Optical Landmark Detection for Spacecraft Navigation," in *Proc. AAS/AIAA Astrodynamics Specialist Conf.,* Springfield, VA, USA, Feb. 2003, Amer. Astronautical Soc. Paper 02-224.

[14] S. Gillam, W. Owen, A. Vaughan, T. Wang, J. Costello, R. Jacobson, D. Bluhm, J. Pojman, and R. Ionasescu, "Optical Navigation for the Cassini/Huygens Mission," *Proc. AAS/AIAA Astrodynamics Specialist Conf.,* Springfield, VA, USA, 2007, Amer. Astronautical Soc. Paper 07-252.

[15] W. Owen, P. Dumont, and C. Jackman, "Optical Navigation Preparations for New Horizons Pluto Flyby," in *Proc. 23rd Int. Symp. Space Flight Dyn. (ISSFD),* Pasadena, CA, USA, Oct. 2012, pp. 1-15. [Online]. Accessed May 2020. Available: https://trs.jpl.nasa.gov/bitstream/handle/2014/42995/12-5363_A1b.pdf?sequence=1&isAllowed=y

[16] J. L. Goodman, "Apollo 13 Guidance, Navigation, and Control Challenges," in *AIAA SPACE 2009 Conf. Expo.,* 2009, doi: 10.2514/6.2009-6455.

[17] J. Christian, "StarNAV: Autonomous Optical Navigation of a Spacecraft by the Relativistic Perturbation of Starlight," *Sensors,* vol 19, no 19, pp. 4064, 2019, doi: 10.3390/s19194064.

[18] J. Christian and S. Robinson, "Non-Iterative Horizon-Based Optical Navigation by Cholesky Factorization," *J Guid Control Dyn,* vol. 39, no. 12, pp. 2755–2765, 2016, doi: 10.2514/1.G000539.

[19] J. Christian, "Optical Navigation Using Iterative Horizon Reprojection," *J Guid Control Dyn,* vol. 39, no. 5, pp. 1092–1103, 2016, doi: 10.2514/1.G001569.

[20] A. Al-Sharadqaha and N. Chernovb, "A doubly optimal ellipse fit," *CSDA,* vol. 56, no. 9, pp. 2771-2781, 2012, doi: 10.1016/j.csda.2012.02.028.

[21] H. Melosh, (2011). "The shapes of planets and moons" in *Planetary Surface Processes,* New York, NY, USA: Cambridge University Press, 2011, pp. 25–48. [Online]. Available: https://doi.org/10.1017/CBO9780511977848. Accessed: May, 2020.

[22] I. Cohen, A. Whitman, and J.Budenz, *The Principia: The Authoritative Translation and Guide: Mathematical Principles of Natural Philosophy,* Los Angeles, CA, USA: University of California Press, 1999. Accessed November 18, 2020. [Online]. Available: http://www.jstor.org/stable/10.1525/j.ctv1xxshj

[23] S. J. Peale, "The Rotation of Hyperion," *The Royal Society,* vol. 313, no. 1524, pp 147-156, 1984, doi: 10.1098/rsta.1984.0090.

[24] J. Wisdom, S. J. Peale, and F. Mignard, "The chaotic rotation of Hyperion," *Icarus,* vol. 58, no. 2, pp. 137-152, 1984, https://doi.org/10.1016/0019-1035(84)90032-0.

[25] B. Smith, et al. "A New Look at The Saturn System: Voyager 2 Images," *Science,* vol. 215, no 4532, pp. 504-537, 1982, doi: 10.1126/science.215.4532.504.

[26] J. Wisdom, "Rotational Dynamics of Irregularly Shaped Natural Satellites," *AJ,* vol. 94, no 5, pp. 1350-1360, 1987, doi: 10.1086/114573.

[27] J. A. Burns and S. J. Weidenschilling, "Side effects of collisions: spin rate changes, tumbling rotation states, and binary asteroids," *Asteroids III,* vol. 1, pp. 517-526, 2002. Accessed Oct. 2020. [Online]. Available: https://www.lpi.usra.edu/books/AsteroidsIII/pdf/3036.pdf

[28] C. Benson, D. Scheeres, and N. Moskovitz, "Spin state evolution of asteroid (367943) Duende during its 2013 earth flyby," *Icarus,* vol 340, 2020. https://doi.org/10.1016/j.icarus.2019.113518.

[29] N. Moskovitz, et. all, "Observational investigation of the 2013 near-Earth encounter by asteroid (367943) Duende," *Icarus,* vol 340, 2020, https://doi.org/10.1016/j.icarus.2019.113519.

[30] Y. Takahashi, M. Busch, and D. Scheeres, "Spin State and Moment of Inertia Characterization of 4179 Toutatis," *AJ,* vol. 146, no 4, pp. 1-10, 2013, doi: 10.1088/0004-6256/146/4/95.

[31] A. Harris, "Tumbling Asteroids," *Icarus,* vol 107, no 1, pp. 209-211, 1994, https://doi.org/10.1016/j.icarus.2004.07.021.

[32] J. Christian, J. Hikes, and L. Benhacine, "Geometric Calibration of the Orion Optical Navigation Camera Using Star Field Images," *AAS Guid., Nav., Control Conf.,* Feb. 2016, American Astronautical Soc. Paper 2016-116, doi: 10.1007/s40295-016-0091-3.

[33] R. Hartley and A. Zisserman, "Action of a Projective Camera on Quadrics," *Multiple View Geometry in Computer Vision,* 2nd ed., New York, NY, USA: Cambridge Univ. Press, 2004, pp. 201–202. [Online]. Available: doi:10.1017/CBO9780511811685. Accessed: May, 2020.

[34] Y. Ma, S. Soatto, J. Košecká, and S. Sastry, *An Invitation to 3-D Vision: From Images to Geometric Models,* New York, NY, USA: Springer, 2010, pp. 49–59. [Online]. Avalable: https://www.eecis.udel.edu/ cer/arv/readings/old_mkss.pdf. Accessed: April, 2020.

[35] D. Eberly, "Reconstructing an Ellipsoid from Its Perspective Projection onto a Plane," GeometricTools.com. https://www.geometrictools.com/Documentation/ReconstructEllipsoid.pdf (accessed May 2020).

[36] J. Christian, "Optical Navigation for a Spacecraft in a Planetary System," Ph.D. Thesis, Univ. of Texas at Austin, Austin, TX, 2010.

[37] J. Christian, "Optical Navigation Using Planet's Centroid and Apparent Diameter in Image," *J Guid Control Dyn,* vol. 38, no. 2, pp. 192–201, Feb. 2015, doi: 10.2514/1.G000872.

[38] Y. Shiu and S. Ahmad, "3D Location of Circular and Spherical Features by Monocular Model-Based Vision," *Inst. of Elect. and Electronics Engineers Conf. Syst., Man and Cybern.,* Piscataway, NJ, 1989, IEEE Publ., doi: 10.1109/ICSMC.1989.71362.

[39] D. Wokes and P. Palmer, "Perspective Reconstruction of a Spheroid from an Image Plane Ellipse," *Int. J. Comput. Vis,* vol. 90, no. 3, pp. 369–379, Dec. 2010, doi: 10.1007/s11263-010-0368-0.

[40] D. Mortari, F. de Dilectis, and C. D'Souza, "Image Processing of Illuminated Ellipsoid," *AAS/AIAA Astrodynamics Specialist Conf.,* 2013, American Astronautical Soc. Paper 2013-853, doi: 10.2514/1.A33342.

[41] J. Christian, "Accurate Planetary Limb Localization for Image-Based Spacecraft Navigation," *J. Spacecr. Rockets,* vol. 54, no. 3, pp.708-727, 2017, doi: 10.2514/1.A33692.

[42] D. Gruber. (Sept 2000). The mathematics of the 3D rotation matrix. Presented at the Xtreme Game Developers Conf.. Accessed: June 2020. [Online]. Available: http://www.fastgraph.com/makegames/3drotation/

[43] J. Christian, "Optical Navigation Using Planet's Centroid and Apparent Diameter in Image," *J Guid Control Dyn,* vol. 38, no. 2, pp. 192-201, 2015, doi: 10.2514/1.G000872.

[44] D. Modenini, "Attitude Determination from Ellipsoid Observations: A Modified Procrustes Problem," *J Guid Control Dyn,* vol. 41, no. 10, pp. 2320-2325, 2015, doi: 10.2514/1.G003610.

[45] R. Halíř and J. Flusser. (Feb. 1998). Numerically Stable Direct Least Squares Fitting of Ellipses. Presented at the 6th Int. Conf. Central Europe Comp. Graph. Visualization. [Online]. Accessed: July 2020. Available: http://autotrace.sourceforge.net/WSCG98.pdf

[46] G. Wabha, "A Least Squares Estimate for Spacecraft Attitude," *SIAM Rev Soc Ind Appl Math,* vol. 7, no. 3, pp. 409–409, 1965, doi: 10.1137/1007077.

[47] F. L. Markley and J. L. Crassidis, "Matrix Solutions of Wahba's Problem," in *Fundamentals of Spacecraft Attitude Determination and Control,* New York, NY, USA: Springer, 2014, pp. 196–197. [Online]. Accessed: May 2020. Available: doi:10.1007/978-1-4939-0802-8.